frontiers | Frontiers in Environmental Science

TYPE Brief Research Report
PUBLISHED 09 December 2024
DOI 10.3389/fenvs.2024.1474608

OPEN ACCESS

EDITED BY
Antonio Donateo,
National Research Council (CNR), Italy

REVIEWED BY
Usman Mazhar,
University of the Punjab, Pakistan
Nicola Paciolla,
Polytechnic University of Milan, Italy

*CORRESPONDENCE
María de la Luz Espinosa-Fuentes,
marilu@atmosfera.unam.mx

RECEIVED 25 September 2024
ACCEPTED 19 November 2024
PUBLISHED 09 December 2024

CITATION
Barrios-Barocio A, Peralta O, Ochoa-Moya CA, Luyando E and Espinosa-Fuentes MdlL (2024) Heat wave: a new characterization in terms of energy.
Front. Environ. Sci. 12:1474608.
doi: 10.3389/fenvs.2024.1474608

Heat wave: a new characterization in terms of energy

Alejandra Barrios-Barocio[1,2], Oscar Peralta[2], Carlos A. Ochoa-Moya[2], Elda Luyando[2] and María de la Luz Espinosa-Fuentes[2]*

[1]Posgrado en Ciencias de la Tierra, Universidad Nacional Autónoma de Mexico, Mexico City, Mexico, [2]Instituto de Ciencias de la Atmósfera y Cambio Climático, Universidad Nacional Autónoma de Mexico, Mexico City, Mexico

Heat waves (HW) are prolonged periods of excessively hot weather that can cause severe socioeconomic and environmental impacts. This study aims to evaluate the differences in stored heat and turbulent flux partitioning during a heat wave event in Mexico City, using observations from an eddy covariance tower during the period from 14 June to 21 June 2023. During this period, net radiation (Rn) and sensible heat flux (H) increased significantly, particularly from noon to evening, reflecting stable atmospheric conditions. The air temperature showed a noticeable increase in the afternoon and evening, whereas absolute humidity decreased. We found that during the heat wave, the Bowen ratio (β) increased by 80% during daylight hours and 65% over a full 24-hour period compared to the pre-heat wave period. This heat release at night prolonged warm conditions, intensifying heat stress. The partitioning of net radiation for latent heat (LE), sensible heat (H), and heat storage (ΔQs) showed significant changes; during the heat wave, 51% of Rn was allocated to H and 34% to ΔQs, compared to pre-heat wave values of 49% and 27%, respectively. This study introduces a new characterization of heat waves in terms of energy, emphasizing the significant shifts in energy flux partitioning and storage. The new characterization highlights the critical role of urban heat storage and its release in exacerbating heat stress during and after heat wave events. This approach provides a comprehensive understanding of the energy dynamics during heat waves, which is essential for developing effective mitigation strategies to combat the adverse effects of extreme heat in urban environments.

KEYWORDS

heat waves, turbulent flux, net radiation, sensible heat flux, heat storage

1 Introduction

Heat waves (HW) are extremely hot weather conditions (Robinson, 2001) that exceed temperature, humidity, and duration thresholds, which can last from days to weeks (Fanta Garuma, 2022). They have socioeconomic and environmental consequences (Meehl and Tebaldi, 2004; Mohammad Harmay and Choi, 2022), produce heat stress, and lead to increased medical conditions and mortality (Fanta Garuma, 2022; Ngarambe et al., 2020) and have impacts on air quality, energy consumption, agricultural production, ecosystem services, and ecosystem productivity (Ao et al., 2019; Li et al., 2015; Peterson et al., 2013).

Urban regions experience warmer conditions than surrounding suburban and rural areas due to the creation of urban heat islands (UHIs) (Founda and Santamouris, 2017; Kong et al., 2021). Among the main factors that promote creation of UHIs is the change in the surface energy balance due to the replacement of natural elements with artificial ones with higher heat absorption and storage capacity, which modify sensible (H) and latent (LE) heat fluxes and reduce evapotranspiration and evaporative cooling rates (Founda and Santamouris, 2017; Khan et al., 2020; Kong et al., 2021; Ngarambe et al., 2020). In addition, the configuration and density of buildings in urban areas often distort wind flow mechanisms, resulting in increased anthropogenic emissions (Khan et al., 2020; Ngarambe et al., 2020).

The change in the surface energy balance and the partitioning of turbulent H and LE fluxes are the effects of the UHIs (Kong et al., 2021; Li et al., 2016). However, there are no conclusive results on the relative change in urban overheating during HWs, so the interaction between both phenomena is an open question (Khan et al., 2020; Kong et al., 2021).

Several authors (Ao et al., 2019; Founda and Santamouris, 2017; Li et al., 2015; Mohammad Harmay and Choi, 2022; Ngarambe et al., 2020) have found synergies between UHIs and HWs, where the lack of surface moisture, anthropogenic emissions, and the morphology of urban areas modify the surface energy balance and exacerbate the effects of UHIs during HWs, increasing UHI magnitudes from 1.5°C to 8°C. Sometimes, the incoming shortwave radiation is found to be increased during HWs due to prevailing high-pressure systems and atmospheric stability (Ao et al., 2019; Matsumura et al., 2015; Meehl and Tebaldi, 2004; Jiang et al., 2019; Li et al., 2015).

The limited vegetation cover, low soil moisture content, and high heat storage capacity of building materials in urban areas lead to a noticeable increase in H and energy storage (ΔQs), as well as a reduction in LE as compared to suburban and rural areas (Ao et al., 2019; He et al., 2020; Kong et al., 2021; Stewart and Oke, 2012). So the extent of urban areas and their building density are crucial factors influencing the UHI intensity during HWs. A higher building density increases the storage of heat that will be released during nights, hinders and modifies the natural wind flow, and reduces energy dissipation, intensifying the UHI effect (An et al., 2020; Founda and Santamouris, 2017; Jiang et al., 2019; Li et al., 2015; Ngarambe et al., 2020; Ramamurthy and Bou-Zeid, 2017).

Even though 75% of the 3 billion urban residents worldwide live in developing countries, only a few measurements of energy and mass fluxes in urban areas have been conducted (Velasco et al., 2005). Some studies quantify the impact of HW events on UHIs through direct measurements in specific areas (Fanta Garuma, 2022), but in tropical urban areas, the information is scarce (Mohammad Harmay and Choi, 2022; Tejeda-Martínez and Jáuregui-Ostos, 2005).

Studies that measure directly and locally the components of the energy balance in Mexico City (Barradas et al., 1999; Oke et al., 1992; 1999) report higher levels of stored heat in areas with low vegetation and high building density, compared to those areas with green areas. For that reason, the objective of this study is to evaluate the differences in stored heat and turbulent flux partitioning (H and LE) during an HW event compared to the periods before and after (PreHW and PostHW) using observations from an eddy covariance tower located in Mexico City.

2 Methods

2.1 Study site

The study site is located at the atmospheric instrumentation platform of the Instituto de Ciencias de la Atmósfera y Cambio Climático (ICAyCC), at the Universidad Nacional Autónoma de México main campus in Mexico City (19.3262°N and 99.1761°W), at an altitude of 2,280 m above sea level. The climate is temperate sub-humid, with rainfall occurring during the summer and two seasons per year: wet season (June to October) and dry season (November to May). The average annual temperature is 15.6°C, with a minimum/maximum temperatures ranging from 14.3°C to 17.4°C, while the average maximum temperature is 26.7°C (reached in May), ranging from 23.2°C to 30.9°C (González Del Castillo et al., 2022).

The ICAyCC is between two contrasting zones in relation to urban surface characteristics and population density. The Universidad Nacional Autónoma de México campus extends to the north, west, and south of the measuring site and is characterized by low-rise buildings interspersed with lawns and patches of native shrub, a variable population, and an urban natural reserve with an area of 237 ha, called Reserva Ecológica del Pedregal de San Ángel, which spreads to the south and southwest and covers one-third of the campus. To the northeast and east, it is characterized as an area with high population density and minimal vegetation, and there is a major public transportation hub and a compact, low-rise or Type III local climate zone (Stewart and Oke, 2012).

According to Stewart and Oke (2012), the UNAM campus falls within the Open Midrise local climate zone, which is characterized by mid-rise buildings (less than seven stories) constructed primarily of concrete, stone, and glass, as well as abundant vegetation cover, mainly low plants and some trees with an average height ranging from 10 to 25 m. The sky view factor ranges from 0.5 to 0.8, indicating the proportion of the sky visible from the ground without building obstructions. The aspect ratio (height-to-width of spaces) varies from 0.3 to 0.75. The built-up area constitutes 20%–40%, the impervious surface fraction is 30%–50%, the vegetative or permeable cover is 20%–40%, and the surface albedo ranges from 0.12 to 0.25.

The northeast and east are characterized as areas with high population density and minimal vegetation, public transportation hubs, and a compact, low-rise or type III local climate zone (Stewart and Oke, 2012) with low-rise buildings ranging from one to three stories and predominantly paved surfaces. The construction materials include concrete, stone, tile, and cement. The sky view factor ranges from 0.2 to 0.6, indicating a limited extent of visible sky unobstructed by buildings. The aspect ratio (height-to-width of spaces) ranges from 0.75 to 1.15. The built-up area covers 40%–70%, the impervious surface fraction is 20%–50%, the vegetative or permeable cover is less than 30%, with an average height ranging from 3 to 10 m, and a surface albedo between 0.1 and 0.2.

2.2 Flux and meteorological measurements

An open-path eddy covariance flux measurement system (EC) was used to measure energy fluxes and meteorological variables directly and continuously throughout June 2023. The EC technique is frequently used to study the exchange of energy, water vapor, CO_2,

volatile organic compounds, and other trace gases over ecosystems (Baldocchi et al., 2001; Schmid, 2000; Velasco et al., 2005; Wilson et al., 2001). The EC setup was installed on an 18-m tower, on the ICAyCC platform, resulting in a total height of 30 m above ground level.

A three-dimensional sonic anemometer (Gill WindMaster Pro, Gill Instruments Ltd.) was used to directly measure horizontal and vertical wind velocity components and sonic temperature. An open-path infrared gas analyzer (IRGA LI-7500A, LI-COR Inc.) was used to measure fluctuations of water vapor and CO_2 concentrations. Both instruments were operated at a sampling frequency of 10 Hz and data collected using a data acquisition system (LI-7550, LI-COR Inc.). A net radiometer (Kipp and Zonen NR-Lite), a quantum sensor (LI-190RS), and a temperature and relative humidity sensor (Vaisala HMP 155A) record net solar radiation (Rn), photosynthetically active radiation (PAR), and air temperature and relative humidity, respectively, all controlled through the Sutron 9210B data logger.

The turbulence data were used to calculate 30-min average fluxes using the LI-COR's EC processor software. The sensible heat vertical flux (H) was determined according to the EC technique as the mean covariance between the instantaneous deviation of the vertical wind velocity (w') and the instantaneous deviation of air temperature from their 30-min means. The latent heat vertical flux (LE) was calculated as the mean covariance between w' and the instantaneous deviation of water vapor in the air on 30-min means.

2.3 Heat wave definition

HWs do not have a common definition accepted by the entire scientific community (Dimitriadou et al., 2021; Meehl and Tebaldi, 2004), and there are several ways to determine the existence of these events (Jáuregui, 2009; Meehl and Tebaldi, 2004; Robinson, 2001; Souch and Grimmond, 2004). In this study, we use the Jáuregui's (2009) definition given for Mexico City, which states that a HW must have a maximum temperature greater than or equal to 30°C, for at least 3 consecutive days and an average temperature greater than or equal to 24°C in the same period.

Given the above definition, in June 2023, a HW was recorded with a PreHW from June 1 to 8, the HW from June 14 to 21, and a PostHW from June 23 to 30. The days from 9 to 13 June and 22 June were considered as transitional days (TOC), as they fulfil only one of the conditions of the (Jáuregui, 2009) definition.

2.4 Energy balance and footprint

The energy balance for an urban surface, neglecting horizontal advection, can be expressed as follows:

$$Rn + AH = H + LE + \Delta Qs,$$

where Rn (W/m^2) is the net radiation flux: $Rn = Sin - Sout + Lin - Lout$ and Sin, $Sout$, Lin, and $Lout$ are the incoming shortwave radiation, outgoing shortwave radiation, incoming longwave radiation, and outgoing longwave radiation, respectively. AH is the anthropogenic heat flux corresponding to the additional energy released by human activities, and ΔQs is the net heat flux stored within the urban volume (in ground, biomass, buildings, *etc.*). For this study, ΔQs was estimated as the residual of the surface energy balance, i.e., Rn-H-LE. AH was not specifically considered as the models used for its estimation often carry considerable uncertainty (Loridan and Grimmond, 2012; Sun et al., 2017). This implies that our estimates of ΔQs are conservative, as AH could be significant under HWs (Sun et al., 2017).

We analyzed changes and variability in net radiation (Rn), sensible heat flux (H), and differences of these variables between periods (ΔRn and ΔH) to evaluate the impact of the HW on the surface energy balance. In addition, we used three indicators to determine variations in energy partitioning: the evaporative fraction EF ($=LE/(H + LE)$), the heat storage coefficient rQs ($=\Delta Qs/Rn$), and Bowen's ratio β ($=H/LE$).

We used the online tool to calculate the flux footprint (Kljun et al., 2015) at https://geography.swansea.ac.uk/nkljun/ffp/www/index.php. This tool employs a dispersion model based on atmospheric turbulence, atmospheric stability, wind speed, and measurement height. It generates contour plots representing the contribution areas from which the measured fluxes originated, and the results indicate the area from which 10% to 90% were measured.

3 Results

The HW was established according to the definition of Jauregui (2009); Rn and H increased, particularly the means of Rn and H were higher than those of the period before and after the HW, from noon to evening (7:00 p.m.) with minimal variability, reflecting stable atmospheric conditions (Figures 1A–C). The air temperature (Ta) presented a significant increase in the afternoon and evening and a decrease in absolute humidity (Figure 1D). Likewise, ΔQs also presented the highest values between 2:00 p.m. and 7:00 p.m. (Figures 1E,F), which may reflect the effect of urban overheating.

EF and β had similar values on HW and PostHW in sunlight hours (when $Rn > 0$), exhibiting a small change on the partitioning of turbulent fluxes (H and LE) (Table 1). During the PostHW, LE was lower with respect to HW, even when precipitation was present; this may be due to the low water availability in urban areas and drought conditions generated by the HW.

Between PreHW and HW, β increased to 80% and 65% in a diurnal ($Rn > 0$) and daily time window, respectively. Likewise, rQs increased markedly during the HW. Considering a magnitude elevation of Rn during this period (Table 1; Figure 1A), an increase in rQs ($=\Delta Qs/Rn$) means that heat storage increased more than Rn; in other words, there was a large energy input, and a greater portion of that energy was stored during the day (Figure 1E). Particularly in the diurnal time window, the increase in Rn for the HW period was 15%, whereas the increase in ΔQs was 46%.

In PreHW, the partitioning values of Rn for LE, H, and ΔQs were 24%, 49%, and 27%, respectively. During the HW, approximately 15% of the daytime Rn ($Rn > 0$) was used for evaporation and the rest for heating the system (Table 1), with 51% and 34% of Rn corresponding, respectively, to H and ΔQs. In PostHW, heat storage ΔQs returned to the Rn ratios observed before the HW;

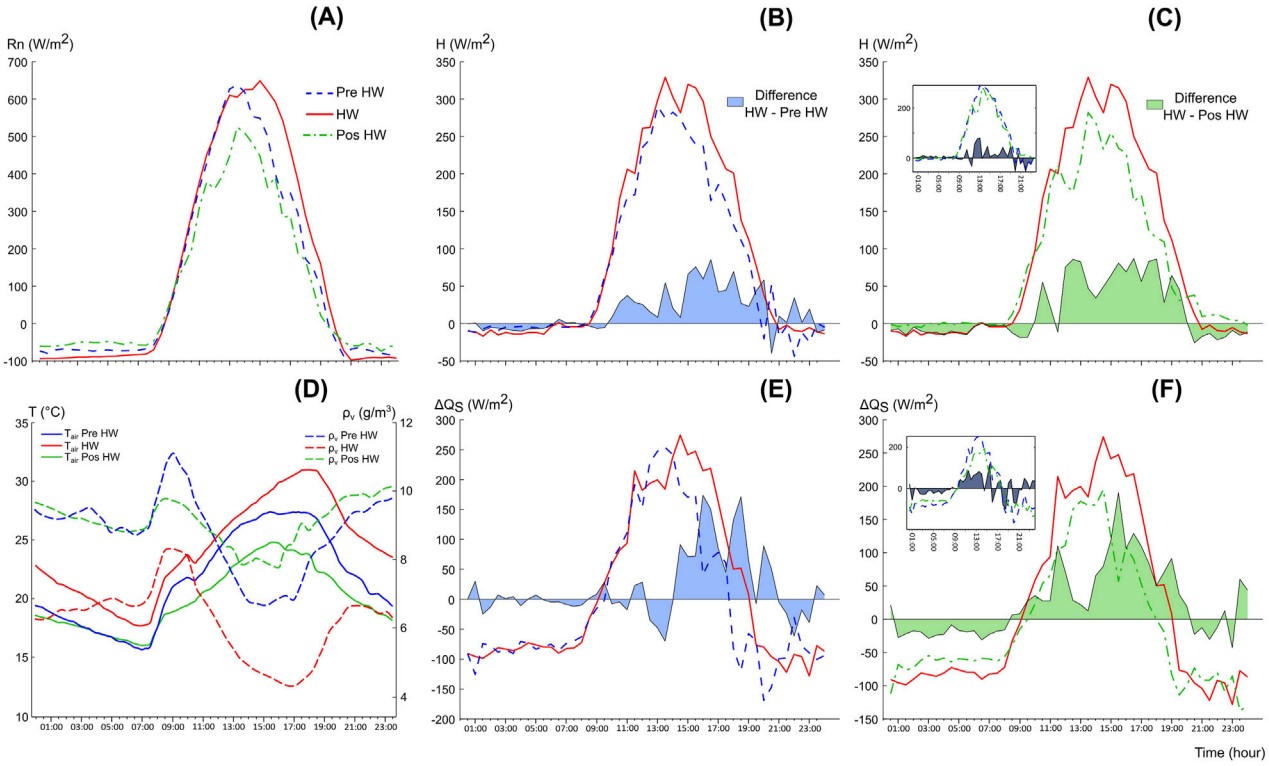

FIGURE 1
Average diurnal cycles of **(A)** net radiation Rn **(B)** and **(C)** sensible heat H and their differences between periods (shaded areas), **(D)** air temperature (solid lines) and absolute humidity (dashed lines), **(E)** and **(F)** energy storage ΔQs and their differences between periods (shaded areas) for PreHW, HW, and PostHW.

TABLE 1 Average diurnal (daytime: Rn > 0) and daily (24 h) flows and flow ratios for the periods before, during, and after the heat wave.

Pre-heat wave period											
	Rn	H	LE	ΔQs	H/Rn	LE/Rn	ΔQs/Rn	β	H/ΔQs	(H+ΔQs)/LE	EF
Daily total	124.13	77.15	51.84	−4.86	0.62	0.42	−0.04	1.49	−15.89	1.39	0.40
Daytime	369.65	182.53	88.10	99.02	0.49	0.24	0.27	2.07	1.84	3.20	0.33
Heat wave period											
	Rn	H	LE	ΔQs	H/Rn	LE/Rn	ΔQs/Rn	β	H/ΔQs	(H+ΔQs)/LE	EF
Daily total	141.94	92.93	34.25	14.77	0.65	0.24	0.10	2.71	6.29	3.14	0.27
Daytime	425.02	216.68	63.56	144.78	0.51	0.15	0.34	3.41	1.50	5.69	0.23
Post-heat wave period											
	Rn	H	LE	ΔQs	H/Rn	LE/Rn	ΔQs/Rn	β	H/ΔQs	(H+ΔQs)/LE	EF
Daily total	99.66	76.40	34.23	−10.97	0.77	0.34	−0.11	2.23	−6.96	1.91	0.31
Daytime	293.68	167.77	50.91	75.00	0.57	0.17	0.26	3.30	2.24	4.77	0.23

notwithstanding the low water availability, the ratio of *H* increased to 57% of Rn at the expense of *ΔQs* (*H/ΔQs =1.50* in HW vs *H/ΔQs =2.24* in PostHW). Given the low evaporation, the major interest was the energy partitioning between *H* and *ΔQs*.

Based on the daily cycles of *Rn*, *H* and *ΔQs* for the PreHW, HW, and PostHW and the respective differences between periods (Figure 1) showed that during the HW, the total increase in *H* relative to the PreHW and PostHW was, respectively, 32% and 81%

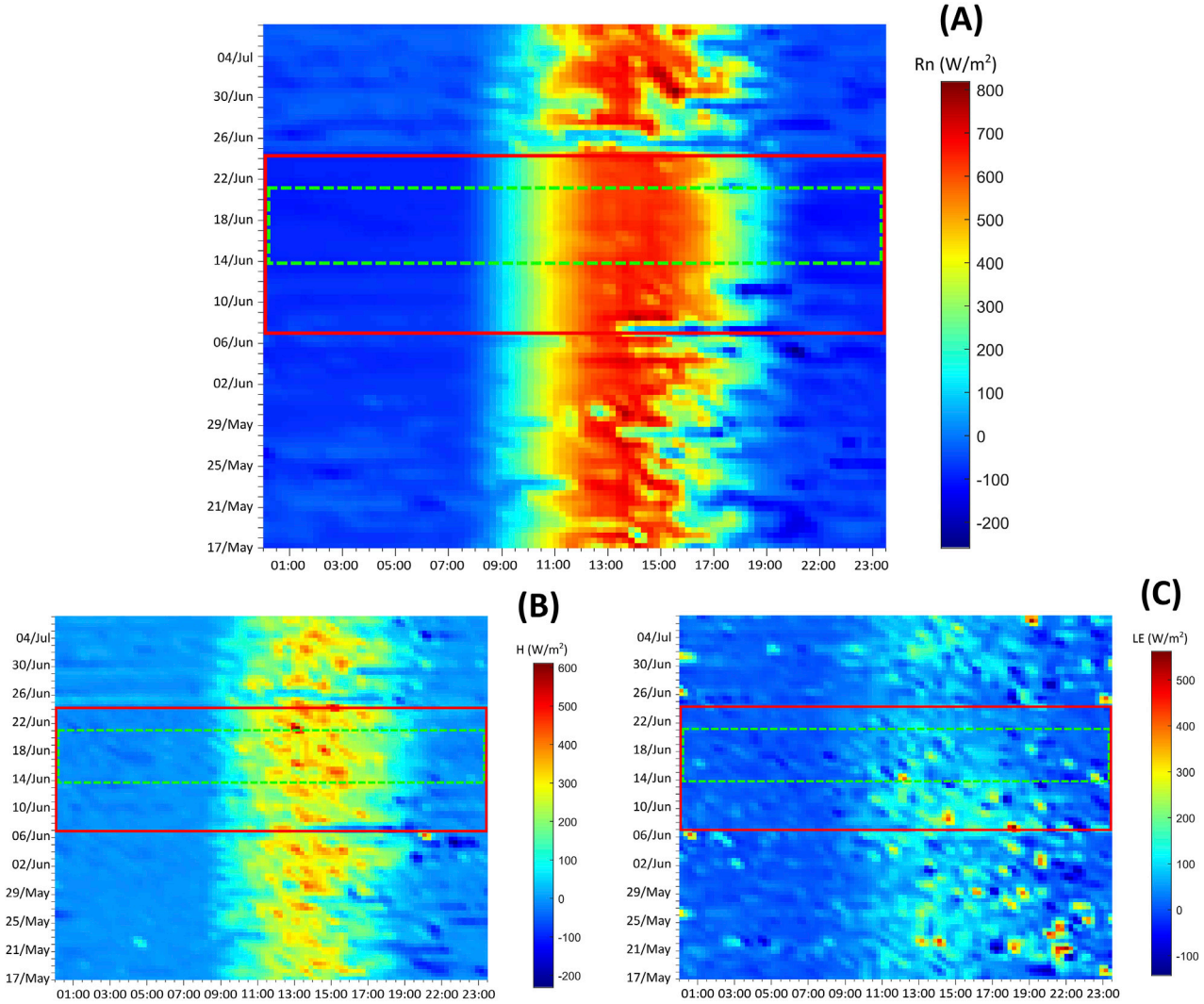

FIGURE 2
Daily cycles of **(A)** Rn, **(B)** H, and **(C)** LE from May 17 to 7 July 2023. The green box corresponds to the heat wave (according to Jáuregui, 2009) from 14 to 21 June 2023. The box Red corresponds to 7 to 24 June 2023.

greater than the difference in *H* between periods not in the HW (*H* PreHW-*H* PostHW, shaded area in the inset plot Figure 1C). Similarly, *ΔQs* increased in total terms by 5% and 21% with respect to the difference in *ΔQs* between periods not in HW (*ΔQs* PreHW–*ΔQs* PostHW, shaded area in the inset plot Figure 1F). On the other hand, taking the total values of *H* and *ΔQs* corresponding to PreHW and PostHW, *H* had an increase of 18% and 31% in the HW period, while *ΔQs* had an increase of 9% and 40%.

In analyzing the behavior of Rn, H, and ΔQs during the heat wave (HW) period, we observed distinct variations in energy fluxes that highlight the impact of atmospheric conditions on energy distribution. Furthermore, examining the spatial extent of the flux footprint provides additional insight into the source area of the measured fluxes over different time periods. The flux footprint indicates that from May 24 to 5 July 2023, the flux originates from an area within the first 166 m from the tower, with occasional extensions up to 384 m. Approximately 70% of the flow comes from an area within 233 m, sometimes extending up to 539 m, and 90% of the flow originates from within 349 m, reaching as far as 700–800 m at times.

During the PreHW period (1 June–8 June 2023), 50% of the flow is captured within the first 170 m, with a maximum range of 340 m; 70% of the flow comes from 238 m, occasionally extending to 476 m, and 90% of the flow originates from within 356 m, with a maximum reach of 714 m. For the HW period (7 June–24 June 2023), the flow footprint shows that 50% of the flow originates from 165 m, extending to 295 m at times; 70% of the flow comes from an area within 231 m, sometimes reaching 413 m, and 90% of the flow originates from within 347 m, with a maximum extension of 618 m. In the Post-HW period (23 June–30 June 2023), 50% of the flow comes from the first 164 m with a maximum reach of 289 m, 70% is captured within 230 m extending up to 406 m, and 90% comes from 344 m, reaching up to 608 m at times. The area of highest contribution to the flow is typically within 130 m of the tower, although the footprint can expand significantly depending on

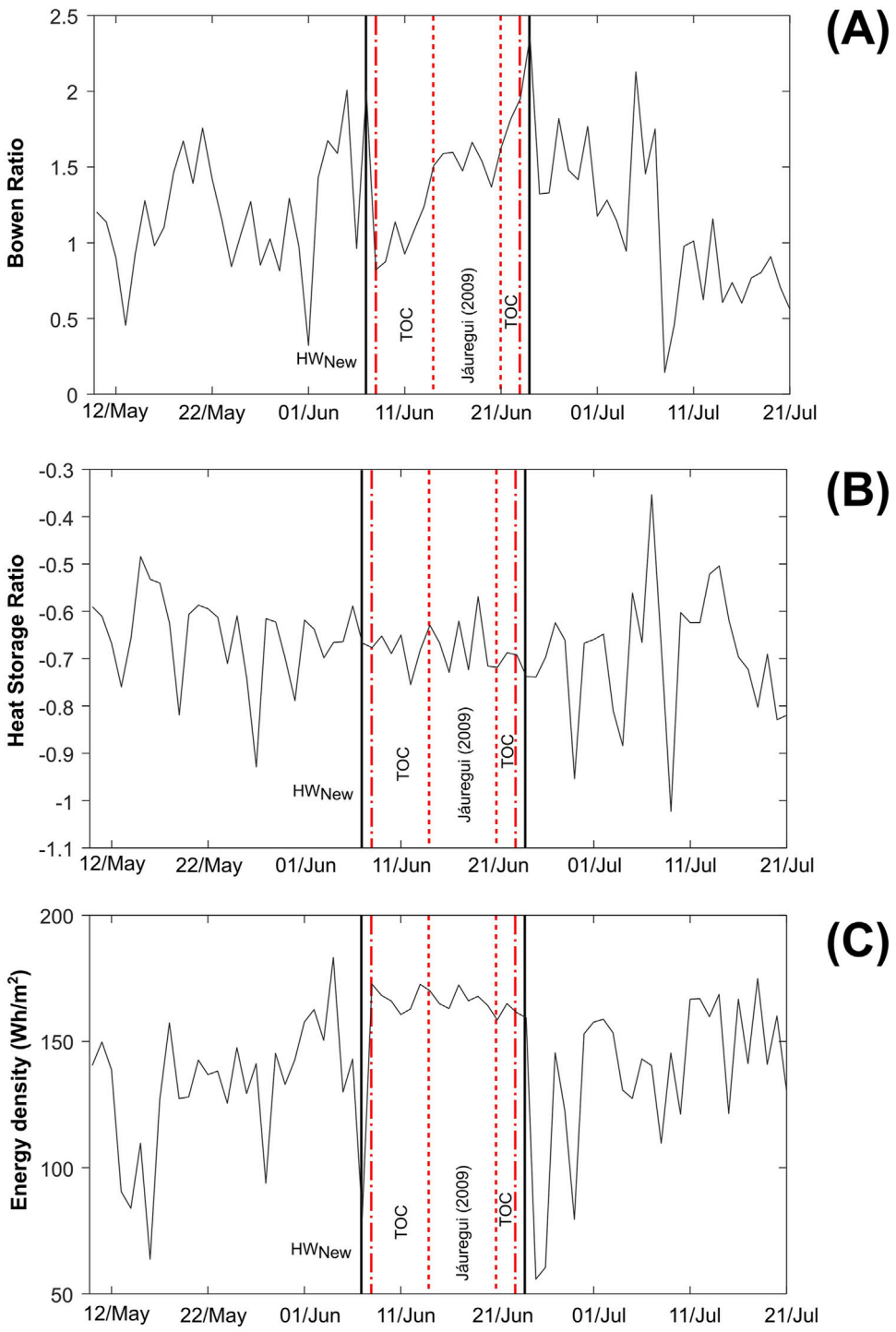

FIGURE 3
Analysis of the coefficient of determination of **(A)** the logarithm of β (Bowen's ratio), **(B)** standard deviation of the logarithm of rQs (heat storage coefficient), and **(C)** energy density (En) from May 10 to 21 July 2023. Red dotted lines correspond to HW (Jauregui, 2009) and TOC's. Black lines delimit HWNew: June 7 to 24, 2023.

atmospheric stability and wind conditions, sometimes extending to several hundred meters (Supplementary Figure S1).

There was a marked change in structure in *Rn* during the period 07/06/2023–24/06/2023, exhibiting greater uniformity of its magnitudes at the same times throughout the period (Figure 2). During the same period, higher *H* magnitudes were maintained for up to 1–1.5 h more in the afternoons than on days outside this period. *LE* increased markedly in the first half of the period and decreased drastically in the second half, which may be due to the minimal water availability at the end of the period.

Correlating the time windows of 3–16 days between May 10 and 21 July 2023, low correlations were obtained at time windows of

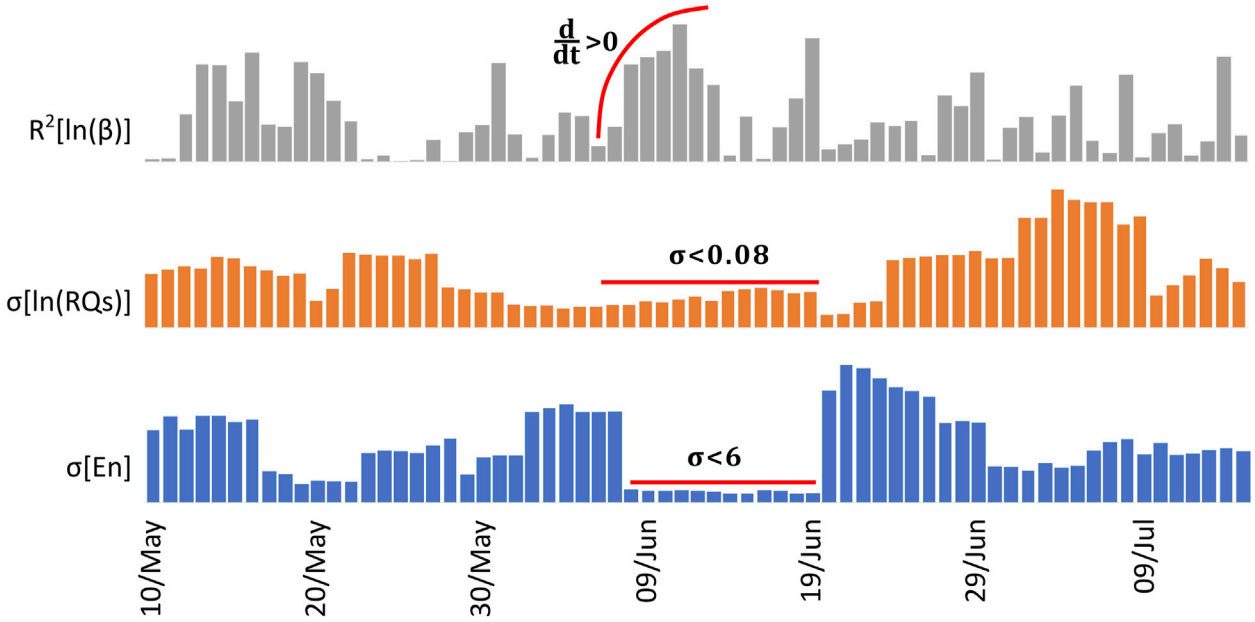

FIGURE 4
Determination coefficient and standard deviation values for logarithms of β, rQs, and energy density (En) from May 10 to 14 July 2023.

4 and 5 days, and a change in the structure in the logarithms of the ratios of the flux amplitudes (*H/LE*, *H/Rn*, *LE/Rn*, and *ΔQs/Rn*) was observed from June 7 to 24, 2023. Based on a time window of 4 and 5 days, we analyzed the coefficient of determination for the linear adjustment of the natural logarithm of *β* and the standard deviation for the natural logarithm of *rQs*, as well as the diurnal energy density (*En = integral of Rn*, *Rn > 0*), from May 10 to 21 July 2023. There was a simultaneous difference in these three parameters from the second day of the HW_{New} (7 June–24 June 2023, bounded by the pair of black lines shown in Figure 3), reflecting a change in diurnal energy density levels, probably due to atmospheric stability and a change in energy partitioning.

4 Discussion

In urban sites, as opposed to rural surfaces, the partitioning of urban canopy energy fluxes can be modified, mainly influenced by the thermal properties of the building material (Christen and Vogt, 2004; Offerle et al., 2006), and the increase in ΔQs can range from 12% to 16% (Newton et al., 2007; Offerle et al., 2006; Callejas et al., 2019). Numerically, H is the most important heat sink in the surface energy balance, ranging from ~40% to 60% of the diurnal Rn (Callejas et al., 2019; Offerle et al., 2003; Grimmond and Oke, 2002), which is consistent with our results.

In this study, flow partitioning with respect to surface characteristics is consistent with that observed in other studies both within and between cities (Grimmond and Oke, 2002; Grimmond et al., 2004). This may be related to the local climate zone type (Stewart and Oke, 2012). However, on a daily basis (full 24-hour period), PreHW and PostHW urban heat storage had a net deficit, indicating that the system cooled on a net basis. In contrast, during the HW, *ΔQs > 0* and *ΔQs/Rn > 0*, meaning that the system warmed in net terms.

The heat release to the atmosphere at night generated heat stress, extending the duration of warm conditions in HW (Sun et al., 2017), and given the low evaporation, the energy was divided between *H* and *ΔQs*. We employed a logarithmic linearization of diurnal cycles (*Rn*, *H*, *LE*, and *ΔQs*) that behaved according to a Gaussian function and determined that the amplitude was susceptible to structure changes in the diurnal cycles during the HW. So, according to Jauregui (2009), the HW and the transition periods (TOC) before and after the HW (Figure 3) are located within the HW_{New}.

Based on the results, we characterized HW in terms of energy under the following conditions (Figure 4):

1) The standard deviation for energy density indicates a lower dispersion, with values below 6 W ($\sigma_{En} < 6W$).

At least one of the following conditions is met within the time frame when the aforementioned event occurs:

a) The derivative with respect to time of the coefficient of determination for ln(β) is positive.
b) The standard deviation for ln(rQs) is less than 0.08.

So, under these terms, a HW occurred from 8 to 20 June 2023.

5 Conclusion

The topography, population, land use, and synoptic weather, among others of a particular region, are relevant in the impact generated by HWs and the response in the local energy balance. Thus, the possible synergies between the effects of UHI and HWs within a given area are distinctive and should be quantified for the areas of interest. To understand these phenomena and their interaction, it is necessary to perform quantitative analyses of the variation of the urban and rural energy balance based on thermal

perturbations and the different local climatic zones. In tropical urban areas, more studies are needed to understand the modulation of the local energy balance and the UHI effect during periods influenced by HWs. In addition to a possible increase in the frequency of HW occurrence because of climate change, it is imperative to carry out studies to determine the possible scenarios that will occur in these regions.

Data availability statement

The original contributions presented in the study are included in the article/Supplementary Material; further inquiries can be directed to the corresponding author.

Author contributions

AB-B: conceptualization, formal analysis, investigation, methodology, writing–original draft, and writing–review and editing. OP: conceptualization, funding acquisition, investigation, supervision, and writing–review and editing. CO-M: Methodology, supervision, validation, and writing–review and editing. EL: methodology, supervision, validation, and writing–review and editing. ME-F: conceptualization, investigation, project administration, supervision, writing–original draft, and writing–review and editing.

Funding

The author(s) declare that financial support was received for the research, authorship, and/or publication of this article. The authors declare financial support was received for the research from PAPIIT-DGAPA, UNAM IN113120.

Acknowledgments

The authors would like to thank the Instituto de Ciencias de la Atmosfera y Cambio Climatico for the facilities provided to the project as well as the Quim. María Isabel Saavedra for her contribution to the revision of the manuscript.

Conflict of interest

The authors declare that the research was conducted in the absence of any commercial or financial relationships that could be construed as a potential conflict of interest.

Publisher's note

Supplementary material

The Supplementary Material for this article can be found online at: https://www.frontiersin.org/articles/10.3389/fenvs.2024.1474608/full#supplementary-material

SUPPLEMENTARY FIGURE S1
(A) Flow footprint for May 24 to 5 July 2023. **(B)** Flow footprint for PreHW (June 1 to 8, 2023). **(C)** Flow footprint for HW (June 7 to 24, 2023). **(D)** Flow footprint for PostHW (June 23 to 30, 2023).

References

An, N., Dou, J., González-Cruz, J. E., Bornstein, R. D., Miao, S., and Li, L. (2020). An observational case study of synergies between an intense heat wave and the urban heat island in beijing. *J. Appl. Meteorology Climatol.* 59 (4), 605–620. doi:10.1175/JAMC-D-19-0125.1

Ao, X., Wang, L., Zhi, X., Gu, W., Yang, H., and Li, D. (2019). Observed synergies between urban heat islands and heat waves and their controlling factors in Shanghai, China. *J. Appl. Meteorology Climatol.* 58 (9), 1955–1972. doi:10.1175/JAMC-D-19-0073.1

Baldocchi, D., Falge, E., Gu, L., Olson, R., Hollinger, D., Running, S., et al. (2001). FLUXNET: a new tool to study the temporal and spatial variability of ecosystem–scale carbon dioxide, water vapor, and energy flux densities. *Bull. Am. Meteorological Soc.* 82 (11), 2415–2434. doi:10.1175/1520-0477(2001)082<2415:FANTTS>2.3.CO;2

Barradas, V. L., Tejeda-Martinez, A., and Jáuregui, E. (1999). Energy balance measurements in a suburban vegetated area in Mexico City. *Atmos. Environ.* 33 (24-25), 4109–4113. doi:10.1016/S1352-2310(99)00152-1

Callejas, I. J. A., Biudes, M. S., Machado, N. G., Durante, L. C., and de Almeida Lobo, F. (2019). Patterns of energy exchange for tropical urban and rural ecosystems located in Brazil central. *J. Urban and Environ. Eng.* 13 (1), 69–79. doi:10.4090/juee.2019.v13n1.69-79

Christen, A., and Vogt, R. (2004). Energy and radiation balance of a central European city. *Int. J. Climatol. A J. R. Meteorological Soc.* 24 (11), 1395–1421. doi:10.1002/joc.1074

Dimitriadou, L., Nastos, P., and Zerefos, C. (2021). Defining heatwaves with respect to human biometeorology. The case of attica region, Greece. *Atmosphere* 12 (9), 1100–1116. doi:10.3390/atmos12091100

Fanta Garuma, G. (2022). How the interaction of heatwaves and urban heat islands amplify urban warming. *Adv. Environ. Eng. Res.* 3 (2), 1–32. doi:10.21926/aeer.2202022

Founda, D., and Santamouris, M. (2017). Synergies between urban heat island and heat waves in athens (Greece), during an extremely hot summer (2012). *Sci. Rep.* 7, 10973. doi:10.1038/s41598-017-11407-6

González Del Castillo, E., Taquet, N., Bezanilla, A., Stremme, W., Ramonet, M., Laurent, O., et al. (2022). CO2 variability in the Mexico City region from *in situ* measurements at an urban and a background site. *Atmósfera* 35 (2), 377–393. doi:10.20937/ATM.52956

Grimmond, C. S. B., and Oke, T. R. (2002). Turbulent heat fluxes in urban areas: observations and a local-scale urban meteorological parameterization scheme (LUMPS). *J. Appl. Meteorology Climatol.* 41 (7), 792–810. doi:10.1175/1520-0450(2002)041<0792:thfiua>2.0.co;2

Grimmond, C. S. B., Salmond, J. A., Oke, T. R., Offerle, B., and Lemonsu, A. (2004). Flux and turbulence measurements at a densely built-up site in Marseille: heat, mass (water and carbon dioxide), and momentum. *J. Geophys. Res. Atmos.* 109 (D24). doi:10.1029/2004jd004936

He, X., Wang, J., Feng, J., Yan, Z., Miao, S., Zhang, Y., et al. (2020). Observational and modeling study of interactions between urban heat island and heatwave in Beijing. *J. Clean. Prod.* 247, 119169. doi:10.1016/j.jclepro.2019.119169

Jáuregui, E. (2009). The heat spells of Mexico City. *Investig. Geográficas* 70, 71–76.

Jiang, S., Lee, X., Wang, J., and Wang, K. (2019). Amplified urban heat islands during heat wave periods. *J. Geophys. Res. Atmos.* 124 (14), 7797–7812. doi:10.1029/2018JD030230

Khan, H. S., Paolini, R., Santamouris, M., and Caccetta, P. (2020). Exploring the synergies between urban overheating and heatwaves (HWs) in western sydney. *Energies* 13 (2), 470. doi:10.3390/en13020470

Kong, J., Zhao, Y., Carmeliet, J., and Lei, C. (2021). Urban heat island and its interaction with heatwaves: a review of studies on mesoscale. *Sustainability* 13 (19), 10923–10932. doi:10.3390/su131910923

Li, D., Sun, T., Liu, M., Wang, L., and Gao, Z. (2016). Changes in wind speed under heat waves enhance urban heat islands in the Beijing metropolitan area. *J. Appl. Meteorology Climatol.* 55 (11), 2369–2375. doi:10.1175/JAMC-D-16-0102.1

Li, D., Sun, T., Liu, M., Yang, L., Wang, L., and Gao, Z. (2015). Contrasting responses of urban and rural surface energy budgets to heat waves explain synergies between urban heat islands and heat waves. *Environ. Res. Lett.* 10 (5), 054009–054010. doi:10.1088/1748-9326/10/5/054009

Loridan, T., and Grimmond, C. S. B. (2012). Characterization of energy flux partitioning in urban environments: links with surface seasonal properties. *J. Appl. Meteorology Climatol.* 51 (2), 219–241. doi:10.1175/JAMC-D-11-038.1

Matsumura, S., Sugimoto, S., and Sato, T. (2015). Recent intensification of the western pacific subtropical high associated with the east asian summer monsoon. *J. Clim.* 28 (7), 2873–2883. doi:10.1175/JCLI-D-14-00569.1

Meehl, G. A., and Tebaldi, C. (2004). More intense, more frequent, and longer lasting heat waves in the 21st century. *Science* 305, 994–997. doi:10.1126/science.1098704

Mohammad Harmay, N. S., and Choi, M. (2022). Effects of heat waves on urban warming across different urban morphologies and climate zones. *Build. Environ.* 209, 108677. doi:10.1016/j.buildenv.2021.108677

Newton, T., Oke, T. R., Grimmond, C. S. B., and Roth, M. (2007). The suburban energy balance in Miami, Florida. *Geogr. Ann. Ser. A, Phys. Geogr.* 89 (4), 331–347. doi:10.1111/j.1468-0459.2007.00329.x

Ngarambe, J., Nganyiyimana, J., Kim, I., Santamouris, M., and Yun, G. Y. (2020). Synergies between urban heat island and heat waves in Seoul: the role of wind speed and land use characteristics. *PLOS ONE* 15 (12), e0243571. doi:10.1371/journal.pone.0243571

Offerle, B., Grimmond, C. S. B., Fortuniak, K., Oke, T. R., and Klysik, K. (2003). "Temporal variability in heat fluxes over a northern European downtown," in Proceedings of 5th International Conference for Urban Climate, Lodz, Poland, 1-5 September, 2003, 1–5.

Offerle, B., Grimmond, C. S. B., Fortuniak, K., and Pawlak, W. (2006). Intraurban differences of surface energy fluxes in a central European city. *J. Appl. Meteorology Climatol.* 45 (1), 125–136. doi:10.1175/jam2319.1

Oke, T. R., Spronken-Smith, R. A., Jáuregui, E., and Grimmond, C. S. B. (1999). The energy balance of central Mexico City during the dry season. *Atmos. Environ.* 33 (24-25), 3919–3930. doi:10.1016/S1352-2310(99)00134-X

Oke, T. R., Zeuner, G., and Jauregui, E. (1992). The surface energy balance in Mexico City. *Atmos. Environ. Part B. Urban Atmos.* 26 (4), 433–444. doi:10.1016/0957-1272(92)90050-3

Peterson, T. C., Heim, R. R., Hirsch, R., Kaiser, D. P., Brooks, H., Diffenbaugh, N. S., et al. (2013). Monitoring and understanding changes in heat waves, cold waves, floods, and droughts in the United States: state of knowledge. *Bull. Am. Meteorological Soc.* 94 (6), 821–834. doi:10.1175/BAMS-D-12-00066.1

Ramamurthy, P., and Bou-Zeid, E. (2017). Heatwaves and urban heat islands: a comparative analysis of multiple cities. *J. Geophys. Res. Atmos.* 122 (1), 168–178. doi:10.1002/2016JD025357

Robinson, P. J. (2001). On the definition of a heat wave. *J. Appl. Meteorology* 40 (4), 762–775. doi:10.1175/1520-0450(2001)040<0762:OTDOAH>2.0.CO;2

Schmid, H. (2000). Measurements of CO2 and energy fluxes over a mixed hardwood forest in the mid-western United States. *Agric. For. Meteorology* 103 (4), 357–374. doi:10.1016/S0168-1923(00)00140-4

Souch, C., and Grimmond, C. S. B. (2004). Applied climatology: 'Heat waves. *Prog. Phys. Geogr. Earth Environ.* 28 (4), 599–606. doi:10.1191/0309133304pp428pr

Stewart, I. D., and Oke, T. R. (2012). Local climate zones for urban temperature studies. *Bull. Am. Meteorological Soc.* 93 (12), 1879–1900. doi:10.1175/BAMS-D-11-00019.1

Sun, T., Kotthaus, S., Li, D., Ward, H. C., Gao, Z., Ni, G.-H., et al. (2017). Attribution and mitigation of heat wave-induced urban heat storage change. *Environ. Res. Lett.* 12 (11), 114007–114009. doi:10.1088/1748-9326/aa922a

Tejeda-Martínez, A., and Jáuregui-Ostos, E. (2005). Surface energy balance measurements in the México City region: a review. *Atmósfera* 18 (1), 1–13.

Velasco, E., Pressley, S., Allwine, E., Westberg, H., and Lamb, B. (2005). Measurements of CO fluxes from the Mexico City urban landscape. *Atmos. Environ.* 39 (38), 7433–7446. doi:10.1016/j.atmosenv.2005.08.038

Wilson, K. B., Hanson, P. J., Mulholland, P. J., Baldocchi, D. D., and Wullschleger, S. D. (2001). A comparison of methods for determining forest evapotranspiration and its components: sap-flow, soil water budget, eddy covariance and catchment water balance. *Agric. For. Meteorology* 106 (2), 153–168. doi:10.1016/S0168-1923(00)00199-4